# Shear banding in soft glassy materials

S. M. Fielding[1]
*Department of Physics, Durham University, Science Laboratories, South Road, Durham, DH1 3LE, UK*

(Dated: 29 April 2014)

Many soft materials, including microgels, dense colloidal emulsions, star polymers, dense packings of multilamellar vesicles, and textured morphologies of liquid crystals, share the basic "glassy" features of structural disorder and metastability. These in turn give rise to several notable features in the low frequency shear rheology (deformation and flow properties) of these materials: in particular, the existence of a yield stress below which the material behaves like a solid, and above which it flows like a liquid. In the last decade, intense experimental activity has also revealed that these materials often display a phenomenon known as shear banding, in which the flow profile across the shear cell exhibits macroscopic bands of different viscosity. Two distinct classes of yield stress fluid have been identified: those in which the shear bands apparently persist permanently (for as long as the flow remains applied), and those in which banding arises only transiently during a process in which a steady flowing state is established out of an initial rest state (for example, in a shear startup or step stress experiment). After surveying the motivating experimental data, we describe recent progress in addressing it theoretically, using the soft glassy rheology model and a simple fluidity model. We also briefly place these theoretical approaches in the context of others in the literature, including elasto-plastic models, shear transformation zone theories, and molecular dynamics simulations. We discuss finally some challenges that remain open to theory and experiment alike.

PACS numbers: 62.20.F,83.10.y,83.60.Wc

## I. INTRODUCTION

Many soft materials, including microgels, dense colloidal emulsions, star polymers, dense packings of multilamellar vesicles, and textured morphologies of liquid crystals, share several notable features in their rheological (deformation and flow) properties. In a steady shear experiment, the 'flow curve' relation $\Sigma(\dot{\gamma})$ between shear stress $\Sigma$ and shear rate $\dot{\gamma}$ is often[1–3] fit to the form $\Sigma - \Sigma_{\rm y} \propto \dot{\gamma}^n$, either with a non-zero apparent yield stress $\Sigma_{\rm y} \neq 0$, or with 'power-law fluid' behaviour for $\Sigma_{\rm y} = 0$. Likewise their viscoelastic spectra, measured in a small amplitude oscillatory shear deformation, exhibit a characteristically flat power-law form over several decades of frequency, even at the lowest frequencies accessible experimentally[4–8]. The same materials often also exhibit rheological ageing[9–13,18–21], in which a sample slowly evolves towards an ever-more solid-like state as a function of its own age: *i.e.,* of the time elapsed since sample preparation.

The widespread observation of these unifying signatures suggests a common cause. Indeed, all these materials share the basic features of structural disorder and metastability. In a dense packing of emulsion droplets, for example, large energy barriers $E \gg k_{\rm B}T$ associated with stretching the interfaces between the droplets impede rearrangements of the droplets relative to one another. In consequence the system may become arrested in disordered, metastable droplet configurations on very long timescales, even if the state of lowest free energy might in principle be ordered. These materials are therefore non-ergodic, and in this sense can be viewed as "glassy". The term "soft glassy materials" (SGMs)[22] has been coined to describe to them.

Beyond the rheological features described above, which have been discussed in detail in previous papers, an accumulating body of experimental data further indicates that heterogeneous "shear banded" flow states often arise when these materials are subject to an imposed shear flow[23–33]. A rich interplay can then take place between this flow heterogeneity that forms on a macroscopic lengthscale, and the material's underlying ageing dynamics. This has a major influence on bulk rheological properties, and so also potentially on any industrial application in which these materials are subject to flow (whether during processing or directly in use), and/or that involve a long shelf life before use.

The aim of this key issues article is to review recent theoretical progress[34–36] in modeling these shear banded flows of densely packed soft glassy materials, as well as of other yield stress fluids such as gels comprising low-density space-spanning networks of attractive colloidal particles. It does so from the particular subjective viewpoint of the "soft glassy rheology" (SGR) model[22], of which this author has the most direct experience. In some places we also supplement our SGR results with studies of a simple "fluidity" model[35]: partly to demonstrate that the phenomena we address are not model-specific, and partly because fluidity models are often more convenient to study numerically.

In a review of this relative brevity it is impossible to describe exhaustively all other theoretical approaches in the literature. Nonetheless, we shall attempt briefly to place our own findings in the context of some other approaches: including shear transformation zone (STZ) theories[37–39], models of coupled elasto-plastic dynamical events[40–46], fluidity models besides the one used here[47,48], and molec-

ular dynamics simulations[49–52]. The reader is encouraged to explore the references provided in these areas.

The manuscript is structured as follows. In Sec. II we survey the experimental evidence for shear banding in soft glassy materials. In Sec. III we describe the SGR and fluidity models. In Secs. IV and V we review recent results for shear banding in soft glassy materials, obtained within these models. Finally in Sec. VI we give conclusions and perspectives for further study.

## II. EXPERIMENTAL MOTIVATION

The rheological properties of yield stress fluids (YSFs) have been intensively investigated during the last decade. In the vicinity of the yield stress, two apparently distinct classes of rheological behaviour have been identified. The first[25,32,53–59] is characterised by a continuous transition between solid-like and liquid-like behaviour as the stress increases above $\Sigma_y$, with the shear rate increasing smoothly from zero as a function of $\Sigma - \Sigma_y$. Associated with this smooth transition in a controlled stress protocol is the observation in slow up/down controlled shear rate sweeps of only minor hysteresis effects[14,55]. Furthermore, under conditions of a constant imposed shear rate, the steady flowing state is one of homogeneous shear for all values of the imposed shear rate, however small. Materials that exhibit these characteristics have come to be termed "simple YSFs" in the literature. Examples include emulsions and carbopol microgels. They typically have predominantly repulsive interactions between their constituent mesoscopic substructures.

A second, contrasting class of rheological behaviour has been identified in YSFs that have attractive interactions between the constituent particles. These materials display a discontinuous transition from solid-like to liquid-like behaviour on increasing the imposed stress above a critical threshold value, with the shear rate jumping discontinuously from zero just below the threshold stress to a finite value $\dot{\gamma}_c$ just above it. Equivalently, the viscosity jumps discontinuously from being effectively infinite (at long times) just below threshold to being finite just above it: an effect referred to as "viscosity bifurcation"[23,48,54,60]. The apparently forbidden window of shear rates $\dot{\gamma} = 0 \to \dot{\gamma}_c$ associated with this jump is then found to correspond, under conditions of a constant imposed shear rate in this range $\dot{\gamma} = 0 \to \dot{\gamma}_c$, to the long time response of the material being shear banded[23–25,30,31].

Associated with this observation of shear banding under conditions of a constant imposed shear rate is the presence in slow up/down shear rate sweeps of strong hysteresis effects [15,30,56,61]. Because of this pronounced hysteresis, materials in this second category are often referred to in the literature as "thixotropic YSFs", in an attempt to distinguish them from the "simple YSFs" discussed above. However even simple YSFs are sometimes seen to show age dependence and shear-rejuvenation (*i.e.*, thixotropy) in their time-dependent flow behaviour[57]. We therefore prefer instead to label these two classes of material as "simple YSFs" and "viscosity-bifurcating YSFs" respectively, and according shall do so throughout the manuscript.

Between these two classes of material, then, only viscosity-bifurcating YSFs appear to display shear banding as their long-time, "permanent" response to a steady imposed shear rate. This permanent banding is then strongly reminiscent of the steady state shear banding that has been intensively investigated in ergodic complex fluids such as polymers[62–65] and wormlike micelles[66–77]. In particular, macroscopic bands of unequal shear rates $\dot{\gamma}_{low}, \dot{\gamma}_{high}$ coexist at a common value of the shear stress, with the relative volume fraction of the bands controlled by a lever rule[31]. The associated signature in the material's bulk rheology is a characteristic plateau in the composite flow curve $\Sigma(\overline{\dot{\gamma}})$ (where $\overline{\dot{\gamma}}$ now denotes the shear rate applied to the sample as a whole, averaged across the bands). Distinct from conventional ergodic fluids, however, in these YSFs the high viscosity band is effectively unsheared, $\dot{\gamma}_{low} \approx 0$, and displays ageing dynamics[15,30,31,61].

In ergodic complex fluids, the criterion for the formation of steady state shear bands is widely known: that the constitutive relation $\Sigma(\dot{\gamma})$ between shear stress and shear rate for an underlying base state of homogeneous shear flow should have a region of negative slope, $d\Sigma/d\dot{\gamma} < 0$. Theories based on this concept of a non-monotonic constitutive curve have likewise been put forward to explain permanent (though ageing) shear bands in viscosity-bifurcating YSFs[37,42,43,46–48], as we shall describe in Sec. V below. Other studies[49–52] suggest alternatively the existence of a static yield stress $\Sigma_{Ys}$ (in well rested samples) below which there exists a branch of zero flow states, with $\Sigma_{Ys}$ exceeding the dynamical yield stress $\Sigma_Y$ as measured in a protocol that instead sweeps the shear rate down towards zero. (That dynamical branch is itself purely monotonic.) This gives rise to a downwards step discontinuity (non-monotonicity) in the material's constitutive properties at $\dot{\gamma} = 0$ (see Fig. 6 below) and again allows a coexistence of an unsheared band with a flowing one. We return in Sec. VI to discuss these studies in relation to those of Sec. V.

In contrast, simple YSFs do not form permanent shear bands under a constant imposed shear rate. However it has recently become apparent that shear banding can arise quite generically in *time-dependent* flow protocols[34,35,78,79], even in materials that have a monotonic $\Sigma(\dot{\gamma})$ and therefore lack the possibility of permanent banding under a steady imposed shear. (This statement in fact applies to all complex fluids, and not just the soft glassy ones of interest here. For a recent study of this issue in polymeric and wormlike micellar fluids, see Ref.[79]) In a shear startup protocol, for example, the (almost ubiquitously observed) signature of an overshoot in the stress startup curve $\Sigma(t)$ is thought to be generically associated with the formation of shear bands. Once

formed, these bands may persist only transiently, or may remain to steady state, according to whether the material's underlying constitutive curve $\Sigma(\dot{\gamma})$ is monotonic or non-monotonic. Likewise in a step stress experiment, the presence of simultaneously upward slope and upward curvature in the material's time-differentiated creep response curve $\dot{\gamma}(t)$ is thought to give rise generically to the formation of shear bands[34].

Consistent with these predictions, experiments have indeed revealed shear banding in YSFs during the time-dependent protocols of step stress and shear startup: both in viscosity-bifurcating YSFs[24], which can then remain shear banded even once the system attains its final steady flowing state, *and* in simple YSFs[32] which by definition recover a homogeneous flow in steady state. We shall now briefly review these experiments, discussing in turn the step stress and shear startup protocols.

Following the imposition of a step stress, the most commonly reported rheological response function is the creep curve $\gamma(t)$ (or its time-differential $\dot{\gamma}(t)$), which describes how the material creeps and (perhaps) eventually flows in response to the applied load. Experimentally, these curves show strikingly similar features across a range of YSFs as diverse as ketchup[80], mustard[80], mayonnaise[80], hair gel[80], carbopol[32,80], a hard sphere colloidal glass[81], carbon black[33,82], thermoreversible gels[16] and a lyotropic hexagonal columnar phase[83], as we shall now describe.

For an applied stress $\Sigma < \Sigma_{\rm y}$, one typically observes a process of very slow creep in which the shear rate progressively tends towards zero at long times, often in the form of a power law $\dot{\gamma} \sim t^{-\beta}$. In contrast, for an imposed stress just above $\Sigma_{\rm Y}$ the strain response typically shows a succession of several distinct regimes. Initially, the material creeps as though at an imposed stress just below yield, with $\dot{\gamma} \sim t^{-\beta}$. (This phenomenon is often referred to as Andrade creep, following original observations by that author in 1910 of tensile creep in metallic wires[84].) This regime of slow creep then terminates at some fluidisation time $\tau_{\rm f} = \tau_{\rm f}(\Sigma - \Sigma_{\rm y})$, when the shear rate suddenly curves upwards and dramatically increases before finally curving downwards onto a steady flowing state of time-independent $\dot{\gamma}_{\rm ss} = \dot{\gamma}_{\rm ss}(\Sigma - \Sigma_{\rm y})$. For stress values approaching the yield from above, $\Sigma \to \Sigma_{\rm y}^+$, one typically finds $\dot{\gamma}_{\rm ss} \to 0$ and $\tau_{\rm f} \to \infty$ for a simple YSF[32]. For viscosity-bifurcating YSFs $\dot{\gamma}_{\rm ss}$ and $\tau_{\rm f}$ should both remain finite as $\Sigma \to \Sigma_{\rm y}^+$ before $\dot{\gamma}_{\rm ss}$ jumps discontinuously to zero below yield. (The actual functional form of the fluidization time versus stress in the vicinity of yield is complicated, varying from material to material and also depending on wall effects.)

In Ref.[32] these bulk creep curves are measured in tandem with spatially resolved flow profiles across the cell following the imposition of a step stress in carbopol microgel (a simple YSF). During the initial phase of slow creep, the shear rate profile remains homogeneous. Subsequently, at the onset of fluidisation, strong wall slip arises that quickly gives way to bulk shear banding as the shear rate increases strongly. The bands then decay as the shear rate curves downwards onto its final steady state value. The eventual steady flowing state is then homogeneous, consistent with carbopol being a simple YSF. Slow creep followed by fluidisation during which shear localisation occurred was also reported in a viscosity-bifurcating YSF in Ref.[33].

In a shear startup experiment, a previously well rested sample is subject for all times $t > t_w$ to shear of constant rate $\dot{\gamma}$, eventually leading to a steady flowing state in the limit $t \to \infty$. Here $t_w$ denotes the time elapsed since sample preparation before the flow commenced. Refs.[55,57] report startup experiments on carbopol, again with spatially resolved velocimetry of the flow profiles across the shear cell reported in tandem with bulk rheological measurements. At early times, the stress startup signal $\Sigma(t)$ grows linearly with strain, $\Sigma = G\gamma = G\dot{\gamma}t$, and the shear field remains uniform across the cell. At longer times the stress shows a strong overshoot, the height of which depends strongly on the sample age $t_w$ before the flow commenced. The stress then falls from this overshoot as it descends to a final steady state. As it does so, pronounced wall slip followed by macroscopic shear banding are observed in the flow profiles. At longer times the bands decay to again leave a homogeneous shear profile in steady state, consistent with carbopol being a simple YSF.

Shear band formation triggered by stress overshoot in shear startup was also reported in a viscosity-bifurcating YSF in Ref.[24]. In that case the bands persist to steady state, consistent with the more complex rheology of viscosity bifurcating YSFs.

## III. SGR AND FLUIDITY MODELS

Having summarised the experimental phenomenology of shear banding in soft glassy materials, we now discuss the two models that we shall use to address it theoretically: the SGR model and a simple fluidity model. We introduce them here in their original form as first put forward in Refs.[22,35]: each with a monotonic constitutive curve, and so capable of addressing only simple YSFs. In Sec. V below we shall introduce a simple modification to the SGR model that captures a non-monotonic constitutive curve and thereby addresses the permanent shear banding seen in viscosity-bifurcating YSFs, with layer normals in the flow-gradient direction. A similar modification to fluidity models, with permanent banding, was discussed earlier in Ref.[47]. We do not address in this work the possibility of transverse banding in which heterogeneity develops in the vorticity direction, which in a glassy system might be expected to be associated with a discontinuous shear thickening transition[85].

### A. Soft glassy rheology model

The soft glassy rheology (SGR) model[22] is based on Bouchaud's model of glassy dynamics[86]. It considers an ensemble of elements undergoing independent activated hopping dynamics among a (free) energy landscape of traps. In the context of a soft glassy material, each element is taken to represent a mesoscopic cluster of, say, a few tens of emulsion droplets. For any such element it is assumed possible to identify local continuum variables of shear strain $l$ and shear stress $kl$, which describe the cluster's state of local elastic deformation relative to a state of locally undeformed equilibrium. Rheology is incorporated by assuming that, between hops, the strain of each element affinely follows the macroscopic flow field to which that region of material is subject: $\dot{l} = \dot{\gamma}$. The stress of the sample as a whole is defined as the average over the local elemental ones: $\sigma = \langle kl \rangle$.

The hopping of any element out of one trap and into another is then identified with a local yielding event in which a cluster of droplets suddenly rearranges into a new configuration locally. In doing so, it is assumed to select a new trap depth at random from a prior distribution $\rho(E) \sim \exp(-E/x_{\rm g})$, and to reset its local strain $l$ to zero. It is these yielding events, then, that confer rheological stress relaxation.

Hops are taken to be dynamically activated, such that an element in a trap of depth $E$ and with local shear strain $l$ has a probability per unit time of yielding given by $\tau^{-1}(E,l) = \tau_0^{-1} \exp\left[-(E - \frac{1}{2}kl^2)/x\right]$. In this way, the element's stored elastic energy $\frac{1}{2}kl^2$ at any instant offsets the trap-depth $E$, leading to a reduced local barrier to rearrangement $E - \frac{1}{2}kl^2$. This leads to rheological shear thinning in the sample as a whole. Because the typical energy barrier $E \gg k_{\rm B}T$, the parameter $x$ is not the true thermodynamic temperature but rather an effective noise temperature that models in a mean field way coupling with other yielding events elsewhere in the sample.

Combined with the exponential prior $\rho(E)$, the exponential activation factor just described ensures (in the absence of flow at least) a glass transition at a noise temperature $x = x_{\rm g}$. For noise temperatures $x < x_{\rm g}$, the model shows a yield stress $\sigma_{\rm y}$ that initially rises linearly with $x_{\rm g} - x$ just below the glass point. In the absence of an imposed flow (or more generally for sample stresses $\sigma < \sigma_{\rm y}$), rheological ageing occurs: following sample preparation at time $t = 0$ by means of a sudden quench from a high initial noise temperature to a value $x < x_{\rm g}$, the system progressively evolves into ever deeper traps as a function of time since preparation. In rheological terms, this corresponds to a growing stress relaxation time $\langle \tau \rangle \sim t$, and so to ever more solid-like response as a function of the sample age. An imposed shear of constant rate $\dot{\gamma}$ can however arrest ageing and rejuvenate the sample to a steady flowing state of effective age $\langle \tau \rangle \sim 1/\dot{\gamma}$

According to the dynamics just described, then, the probability $P(E,l,t)$ for an element to be in a trap of depth $E$ and with local shear strain $l$ obeys

$$\dot{P}(E,l,t) + \dot{\gamma}\frac{\partial P}{\partial l} = -\frac{1}{\tau(E,l)}P + Y(t)\rho(E)\delta(l). \quad (1)$$

The convected derivative on the left hand side describes affine loading of each element by shear. The first and second terms on the right hand side describe hops out of and into traps respectively, with an ensemble average hopping rate

$$Y(t) = \int dE \int dl \frac{1}{\tau(E,l)} P(E,l,t). \quad (2)$$

The macroscopic stress

$$\sigma(t) = \int dE \int dl\; klP(E,l,t). \quad (3)$$

Throughout we use units in which $\tau_0 = 1$, $k = 1$ and $x_{\rm g} = 1$.

Numerical results for the SGR model's flow curves[87] $\sigma(\dot{\gamma})$ are shown in Fig. 1 for a range of noise temperatures $x$. For $x \geq 2$ these display Newtonian response with $\sigma \sim \dot{\gamma}$; for $1 < x < 2$ we see power-law fluid behaviour with $\sigma \sim \dot{\gamma}^{x-1}$; and for $x < 1$ a non-zero yield stress with $\sigma - \sigma_{\rm y}(x) \sim \dot{\gamma}^{1-x}$.

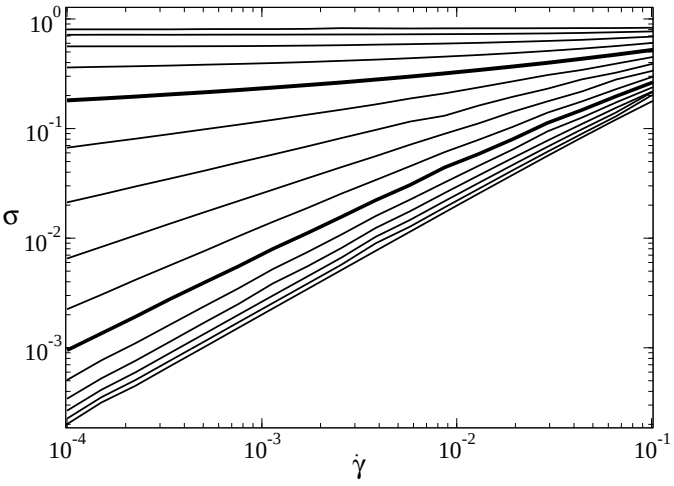


FIG. 1. Constitutive curves of the SGR model for noise temperatures $x = 0.2, 0.4 \cdots 3.0$ (curves downward). Bold lines highlight $x = 1$ and $x = 2$.

So far, we have described the SGR model in its original form as introduced in Ref.[22]. In this form, the model contains no spatial information about the location of any element and, as such, is obviously incapable of addressing shear banded flows in which the flow state of the material varies in the flow-gradient direction $y$. In Ref.[36], therefore, we extended the model to allow spatial variations in this dimension $y$ (with translational invariance still assumed in the flow direction $x$ and vorticity direction $z$). To do so we discretized the $y$ coordinate into $i = 1 \cdots n$ streamlines of equal spacing $L_y/n$, giving an

overall sample thickness $L_y$. For convenience we adopted periodic boundary conditions such that $i = 1, n$ are also neighbours. Each streamline is then assigned a separate ensemble of $j = 1 \cdots m$ SGR elements, with a streamline shear stress $\sigma_i = (k/m) \sum_j l_{ij}$.

In the creeping flow conditions of interest here, the force balance condition decrees that the shear stress is uniform across all streamlines, $\sigma_i(t) = \sigma(t)$. During intervals in which no jump occurs anywhere in the system, the material clearly deforms as a linear elastic solid with $\dot{l} = \dot{\gamma}$ for every element on all streamlines: any stress change is uniform across all streamlines, consistent with force balance. Supposing a hop then occurs at element $ij$ when its local strain is $l = \ell$. (Numerically, we handle the hopping dynamics by a waiting-time Monte Carlo algorithm that stochastically chooses both the element and time of the next hop.) This clearly reduces the stress on that streamline, in potential violation of force balance. By updating all elements on the same streamline $i$ as $l \to l + \ell/m$, force balance then is restored across the streamlines, but (incorrectly) with a stress level that has not been properly reduced by the yielding event. Further updating all elements on all streamlines throughout the system as $l \to l - \ell/mn$ restores the global stress to the properly reduced level.

This algorithm can be thought of as the $\eta \to 0$ limit of a situation in which a small Newtonian viscosity $\eta$ is present alongside the elastic stress of the SGR elements, with local strain rates set to maintain a uniform total stress $\Sigma(t) = \sigma(y,t) + \eta\dot{\gamma}(y,t)$ across the sample at all times, in accordance with the force balance condition. For the long timescales $\tau \gg \eta/k$ and low flow rates $\dot{\gamma} \ll k/\eta$ of interest here, taking this limit $\eta \to 0$ upfront is an excellent approximation.

Finally, a small diffusivity of stress[88] between neighbouring streamlines is needed to ensure that the interface between any shear bands has a slightly diffuse width, rather than being an unphysical step discontinuity. This is incorporated by further adjusting the strain of three randomly chosen elements on each adjacent streamline $i\pm1$ by $\ell w(-1, +2, -1)$, after a hop as described above on streamline $i$. For the small values of the coupling strength $w$ of interest here this mildly changes the model's flow curves relative to those in Fig. 1, but without changing their overall shape.

### B. Fluidity model

In the previous subsection we introduced the SGR model, which considers an ensemble of elastic elements undergoing activated hopping dynamics among an energy landscape of traps, with the probability $P(E, l, t)$ of finding an element in a trap of depth $E$ and with a shear strain $l$ evolving according to Eqn. 1. Out of this full probability distribution one can then define a hierarchy of moments

$$P_{p,q} = \int_{-\infty}^{\infty} dl \int_0^{\infty} dE \, \frac{l^p}{\tau^q} P(E,l,t) \;\text{ for }\; p,q = 0,1,2\cdots, \tag{4}$$

and it is easy to show that these evolve according to

$$\dot{P}_{p,q} = \dot{\gamma} p P_{p-1,q} + \frac{\dot{\gamma} q}{x} P_{p+1,q} - P_{p,q+1} + \frac{1}{1+q/x} P_{0,1}\delta_{p,0}. \tag{5}$$

To fully solve the SGR model's dynamics in this representation, one would of course need to evolve this infinite hierarchy of coupled moments.

In this section we introduce a simplified "fluidity" description, motivated by the momentwise representation of the full SGR model just described[35], and along the lines of earlier fluidity models in Refs.[23,47]. It considers just two moments: the macroscopic stress $\sigma = P_{1,0}$ and the average hopping rate $Y = P_{0,1}$. The latter of these is often termed the material's fluidity, and in fact we further cast it in terms of the material's overall structural relaxation timescale, denoted $\tau \equiv 1/Y$. (The overall $\tau$ defined here is of course distinct from, though related to, the local elemental ones of the full SGR model above.) The fluidity model then directly writes down equations of motion for these two moments, in a form that is loosely inspired by the SGR dynamics for $\dot{P}_{1,0}$ and $\dot{P}_{0,1}$ as given by Eqn. 5 above, but without attempting self consistent closure with regards the other moments.

To set up the fluidity model, then, we decompose the total shear stress in any fluid element into a viscoelastic contribution $\sigma$, and a small Newtonian contribution:

$$\Sigma(t) = \sigma(y,t) + \eta\dot{\gamma}(y,t). \tag{6}$$

As in the SGR model above, we shall be interested in the limit in which the Newtonian contribution acts to ensure force balance on a short timescale set by $\eta$, but otherwise makes negligible contribution.

The dynamics of the viscoelastic contribution to the stress is prescribed by a Maxwell-like model

$$\partial_t \sigma(y,t) = G\dot{\gamma} - \frac{\sigma}{\tau}, \tag{7}$$

describing elastic loading with a modulus $G$, and viscoelastic relaxation on a timescale $\tau$. The relaxation timescale $\tau$ is then assigned its own dynamics

$$\partial_t \tau(y,t) = 1 - \frac{\tau}{\tau_0 + 1/\dot{\gamma}}. \tag{8}$$

In the absence of flow this gives rheological ageing with a growing stress relaxation time $\tau \sim t$: the material evolves towards a progressively more solid-like and less fluid-like state as a function of its own age, following sample preparation assumed to take place via a deep quench at time $t = 0$, such that $\tau(y, t = 0) = \tau_0$. Conversely, under an imposed shear at a constant rate $\dot{\gamma}$, ageing is cutoff at an effective sample age $\tau = \tau_0 + 1/\dot{\gamma}$. The steady state flow curve is then

$$\Sigma = G(1 + \dot{\gamma}\tau_0) + \eta\dot{\gamma}, \tag{9}$$

rising monotonically in $\dot{\gamma}$ beyond a yield stress $\Sigma_y = G$.

Finally we add to Eqn. 8 a diffusive term $l_0^2 \partial_y^2 \tau$ to give a small coupling between streamlines[88] and confer on the interface between bands a slightly diffuse width $O(l_0)$. Throughout we use units in which $G = 1$, $\tau_0 = 1$, and the width of the flow domain $L_y = 1$.

In the next two sections in turn we shall consider the predictions of the SGR and fluidity models for the shear banding behaviour of simple YSFs and (with a simple modification to account for a non-monotonic constitutive curve) viscosity-bifurcating YSFs.

## IV. SIMPLE YIELD STRESS FLUIDS

For a complex fluid subject to a steady imposed shear flow, the criterion for the formation of shear bands that will persist 'permanently' – *i.e.,* for as long as the flow remains applied – is well known: that the constitutive relation $\Sigma(\dot{\gamma})$ between shear stress $\Sigma$ and shear rate $\dot{\gamma}$ for an underlying base state of homogeneous flow has a region of negative slope, $d\Sigma/d\dot{\gamma} < 0$. This criterion is universal to all complex fluids and applies not only to the non-ergodic soft glassy materials of interest here, but also to ergodic fluids such as polymers and wormlike micellar surfactants. In the context of a soft glass with a yield stress, it corresponds to a constitutive curve of the shape in Fig. 4a) below. In their form as described above, however, the SGR and fluidity models have monotonic constitutive curves and are unable to address the permanent banding seen under conditions of a steady applied flow in viscosity-bifurcating YSFs. We shall nonetheless return in Sec. V below to discuss a simple modification to the SGR model that does allow permanent banding.

Besides steady shear, many practical flow situations involve a strong time dependence, whether perpetually or during the transient process whereby a steady flowing state is established in an sample that was previously well rested. Commonly studied protocols include step stress, step strain, and shear startup. In recent years a body of experimental data has accumulated to show that, in many complex fluids, pronounced shear banding can arise during these time-dependent flow protocols, even if the eventual steady flowing state is unbanded. This has been observed in the non-ergodic soft glassy materials of interest here, as surveyed in Sec. II above, as well as in polymeric fluids. (See Ref.[79] and references therein to the experimental polymer literature in this area.)

Motivated by these observations, in a recent Letter[34] we derived criteria for the onset of linear instability to the formation shear bands in time-dependent flows, one for each protocol in turn: step stress, shear startup, and step strain. Importantly, each criterion depends only on the shape of the experimentally measured rheological response function for that protocol, but is otherwise *independent* of the constitutive properties of the particular fluid in question. In this way the criteria apply universally to all complex fluids and have the same highly general status as the widely known criterion for permanent banding in steady shear (of a negatively sloping constitutive curve).

In the next two subsections we discuss the application of these criteria to the onset of shear banding in time-dependent flows of soft glassy materials, with supporting numerical evidence provided by simulating the SGR and fluidity models. A counterpart investigation in the context of polymeric fluids (polymer solutions, polymer melts and wormlike micellar surfactants) was recently performed in Ref.[79], with supporting numerical evidence from the rolie-poly and Giesekus constitutive models.

These predictions for the onset of banding in time-dependent flows are in fact expected to apply to both simple YSFs and viscosity-bifurcating YSFs, given that the instability criteria are universal in the way just described. However the focus in this section is on simple YSFs, for which they have been investigated most thoroughly experimentally, and to which the SGR model in its original form applies. Accordingly, the time-dependent bands predicted in this section always decay to leave homogeneous flow in steady state, consistent with the behaviour of a simple YSF. In a viscosity bifurcating fluid we would expect onset in the same way as predicted here following a step stress or shear startup, but with the bands persisting permanently for applied shear rates $\dot{\gamma} < \dot{\gamma}_c$.

### A. Step stress protocol: slow creep and fluidisation

Consider an experimental protocol in which a sample is freshly prepared in a reproducible state at some time $t = 0$, for example by loading into a rheometer and pre-shearing, then left to age in the absence of any applied flow or loading during a waiting time $t_w$. At this time it is suddenly subject to a step shear stress of size $\Sigma_0$, which is held fixed for all subsequent times:

$$\Sigma(t) = \Sigma_0 \Theta(t - t_w). \tag{10}$$

The relevant rheological response function is then the creep curve $\overline{\gamma}(t - t_w, t_w, \Sigma_0)$, which reports the accumulated strain as a function of the time $t - t_w$ since load application, for any given waiting time $t_w$ and stress amplitude $\Sigma_0$. In the literature the results are often in fact instead reported in terms of the time-differentiated creep (shear rate) curves $\overline{\dot{\gamma}}(t - t_w, t_w, \Sigma_0)$, where the overdot denotes differentiation with respect to $t$.

Experimentally, such curves are measured by recording the motion of the rheometer plates relative to each other and so represents the strain response of the material averaged over the sample as a whole. In any regime where the deformation remains uniform across the sample, it clearly also corresponds to the strain $\gamma(y) = \overline{\gamma}$ at each point locally across the gap. Indeed a commonly made assumption in the literature is that the deformation will remain uniform.

As surveyed in Sec. II, however, many soft glasses in fact form heterogeneous shear banded states as they

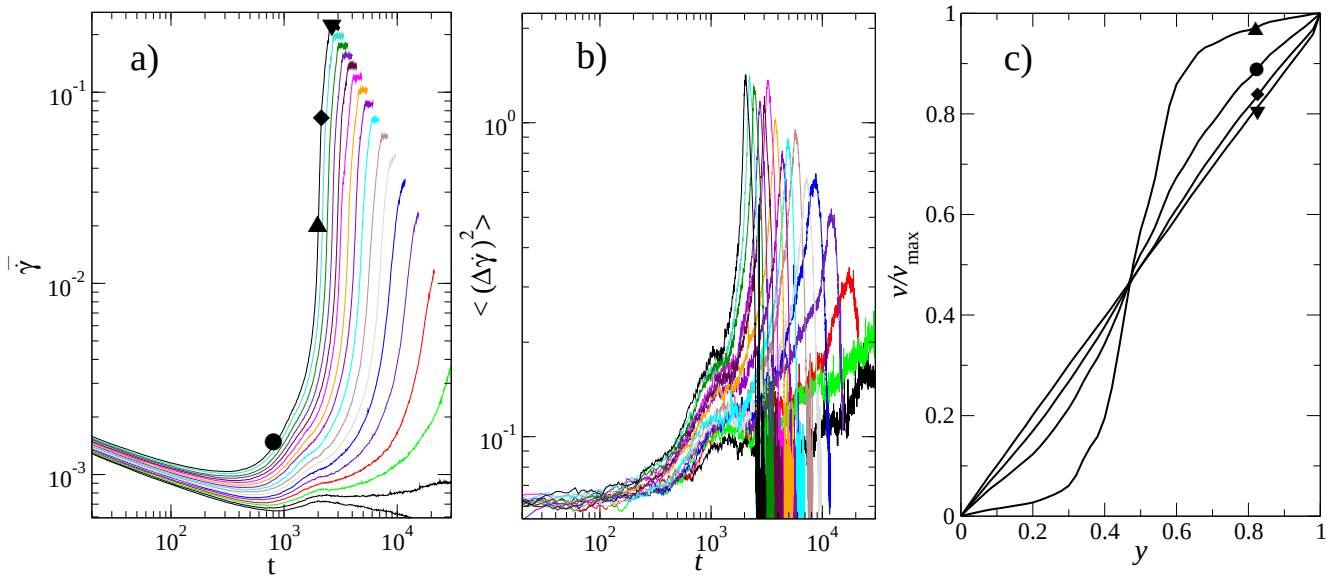


FIG. 2. a) Time-differentiated creep curves of the SGR model for stress values $\Sigma_0/\Sigma_y = 1.005, 1.010 \cdots 1.080$ (curves upwards). b) Corresponding degree of shear banding. c) Normalised velocity profiles at times denoted by corresponding symbols in a) Parameters: $x = 0.3, w = 0.05, n = 50, m = 10000$. Initial sample age $t_w = 10^3\,[1 + \epsilon\cos(2\pi y)]$, $\epsilon = 0.1$.

creep in response to an applied shear stress. Motivated by this observation (and similar ones in polymeric fluids), in Refs.[34,79] we performed an analytical calculation to determine whether (and when) a state of initially homogeneous creep response might become linearly unstable to the formation of shear bands. Doing so, we found the criterion for the onset of banding to be:

$$\frac{\partial^2\bar{\dot{\gamma}}}{\partial t^2}\Big/\frac{\partial\bar{\dot{\gamma}}}{\partial t} > 0. \qquad (11)$$

We argued that this criterion applies universally to all complex fluids, including the soft glassy materials of interest here. In this way, any state of initially homogeneous creep is predicted to become linearly unstable to the formation of shear bands if its time-differentiated creep response curve $\bar{\dot{\gamma}}$ simultaneously shows upward curvature and upward slope as a function of time. (In principle it might instead show downward curvature and downward slope, but we have never in practice seen this in our numerical studies of soft glasses or polymeric fluids.)

This criterion is derived by means of a linear stability analysis that considers an underlying base state of initially homogeneous creep response to the applied load, with strain $\gamma_0(t)$ and strain rate $\dot{\gamma}_0(t)$. (For notational convenience we suppress the $t_w$ and $\Sigma_0$ dependencies in writing these quantities here.) To this base state is added small heterogeneous perturbations to give $\dot{\gamma}(y,t) = \dot{\gamma}_0(t) + \sum_n \delta\dot{\gamma}_n(t)\exp(in\pi y/L_y)$. (Other relevant variables in the equations of motion are treated in the same way, but we do not discuss these details here.) The dynamics of the perturbations are then studied at linear order in their amplitude. The regime in which they are found to grow as a function of time, indicating the onset of shear banding, is found to correspond to that in which the base state strain rate $\dot{\gamma}_0$ obeys (11) above.

As such, then, (11) technically applies to the base state shear rate $\dot{\gamma}_0$ rather than the spatially averaged signal $\bar{\dot{\gamma}}$ as measured experimentally by recording the motion of the rheometer plates. However $\dot{\gamma}_0$ and $\bar{\dot{\gamma}}$ must clearly coincide in any regime before any significant banding arises. To determine the onset of banding, therefore, (11) can be applied to the experimentally measured signal $\bar{\dot{\gamma}}$ direct. In this way, bulk rheological data can be used as a predictor of shear banded flow states, even in the absence of spatially resolved velocimetry.

Having introduced an onset criterion that we suggest applies to all complex fluids, we now consider its implications for the soft glasses of interest here, as modelled by the SGR model in its original form, which we expect to capture the behaviour of simple YSFs. As just argued above, the time-evolution of an underlying homogeneous flow state can be used to predict the onset of banding. We shall therefore first summarise the creep response of the SGR model in its original form[78], which addresses homogeneous flows only, as a natural starting point from which to then understand the shear banding dynamics of the spatially aware model[36].

We focus on noise temperatures in the glass phase $x < x_g$, where the model shows a non-zero yield stress $\Sigma_y(x)$. Following the application of a step stress of

amplitude $\Sigma_0 < \Sigma_y$ below the yield stress and not too close to it, the system responds by a process of slow creep with a logarithmically increasing strain $\gamma_0 \sim A(\Sigma_0)\log[(t-t_w)/t_w]$. The corresponding strain rate accordingly tends towards zero at long times, $\dot{\gamma}_0 \sim A(\Sigma_0)(t-t_w)^{-1}$, with the material creeping ever more slowly as a function of the time since the load was applied. For stress values approaching the yield stress from below the prefactor $A(\Sigma_0)$ becomes very large, with an apparent divergence as $\Sigma_0 \to \Sigma_y$ signifying a crossover to a regime in which the strain no longer behaves logarithmically[89]. However the strain rate nonetheless still progressively evolves towards zero at long times. For applied stress values below the yield stress, then, the strain rate never satisfies (11) and the creep response is predicted to remain homogeneous at all times, even in a spatially aware model that could in principle display banding.

For applied stresses just above the yield stress the system initially responds in a fashion similar to that for stresses just below yield, in the sense that it creeps progressively more slowly over time: here one numerically observes[78] $\dot{\gamma}_0 \sim t_w^{-1}\left[(t-t_w)/t_w\right]^{-x}$. However because the applied stress now exceeds the yield stress, the system must eventually make a transition to a flowing state with a steady state shear rate prescribed by the flow curve, $\dot{\gamma}_0 \sim (\Sigma - \Sigma_y)^{1/(1-x)}$. Indeed we find that this transition occurs via a process of rather sudden fluidisation in which the strain rate (i) curves upwards to increase from the small value it had attained by the end of the slow creep regime, then (ii) goes through an inflexion point, before finally (iii) curving downwards to attain its ultimate value on the flow curve. (Taking the inflexion point as a good measure of the fluidisation time, numerically one finds[78] for the SGR model $\tau_{\text{fluidisation}} \sim t_w(\Sigma - \Sigma_y)^{-\alpha}$ with $\alpha = O(1)$. As noted above, however, experimentally the actual functional form of $\tau_{\text{fluidisation}}(\Sigma - \Sigma_y)$ is found to vary from material to material.) Creep curves of this shape have been observed experimentally in a host of complex fluids, including mayonnaise[80], hair gel[80], carbopol[32,80], a hard sphere colloidal glass[81], carbon black[82] and a lyotropic hexagonal columnar phase[83].

During part (i) of this fluidisation process the strain rate $\dot{\gamma}_0$ simultaneously shows upward slope and upward curvature as a function of time. It therefore satisfies (11), leading us to predict that the spatially aware version of the model should become linearly unstable to the onset of shear banding in this regime. We explored this prediction by performing a full nonlinear simulation of the spatially aware model[34]. This simulation captures not only the initial onset of banding predicted by the linear instability criterion (11), which applies while any heterogeneous perturbations remain small, but also nonlinear effects once the heterogeneity becomes significant in the later stages of band development.

The results are shown in Fig. 2. The left panel shows the time evolution of the strain rate signal $\bar{\dot{\gamma}}$, spatially averaged across the sample. As argued above, this spatially averaged quantity must coincide with the counterpart signal $\dot{\gamma}_0$ of the homogeneous model in any regime before appreciable banding arises. In fact our numerics further show it to agree in overall shape even once banding has set in, following the form described above for $\dot{\gamma}_0$ throughout its full evolution: a prolonged regime of progressively slowing creep is followed by a sudden process of fluidisation with features (i) to (iii) above, with the time of fluidisation apparently diverging as the applied stress value approaches the yield stress from above.

In regime (i) of this fluidisation process, in which the shear rate $\bar{\dot{\gamma}}$ simultaneously shows upward slope and upward curvature, significant shear banding indeed arises, consistent with (11). See the middle panel of Fig. 2, which shows the evolution of the variance in shear rate spatially across the gap as a function of time. This grows markedly in regime (i), then decays after the inflexion point (ii) once the shear rate signal curves downward in regime (iii). Snapshot velocity profiles at the times indicated by the circles in the left panel are given in the right hand panel, and indeed exhibit pronounced shear banding. These predictions of transient banding following fluidisation after a process of slow creep are consistent with experimental observations in Refs.[32,56,57], as discussed in Sec. II above.

### B. Shear startup protocol: stress overshoot

Consider now an experiment in which a sample is freshly prepared at time $t = 0$, left to age in the absence of any applied flow or loading during a waiting time $t_w$, then for all subsequent times subject to shear of constant rate $\dot{\gamma}_0$:

$$\dot{\gamma}(t) = \dot{\gamma}_0 \Theta(t - t_w). \tag{12}$$

The relevant rheological response function is then the stress startup curve $\Sigma(t - t_w, t_w, \dot{\gamma}_0)$ reported as a function of the time $t - t_w$ since shearing commenced, for a given waiting time $t_w$ and shear rate $\dot{\gamma}_0$. Equivalently one may instead report this as a function of the accumulated strain $\gamma_0 = \dot{\gamma}_0(t - t_w)$, again for fixed $t_w$ and $\dot{\gamma}_0$, to give $\Sigma(\gamma_0, t_w, \dot{\gamma}_0)$. For notational convenience in what follows we shall suppress the $t_w$ dependence in writing this, so for any initial sample age $t_w$ we have $\Sigma(\gamma_0, \dot{\gamma}_0)$.

In the context of shear banding, a familiar thought experiment is then to consider a startup flow that is (artificially) constrained to remain homogeneous until a stationary state is attained in the limit $\gamma_0 \to \infty$. In this limit the total accumulated strain becomes irrelevant, as does the waiting time $t_w$, and the stress depends only on strain rate, via the underlying homogeneous constitutive curve $\Sigma(\gamma_0 \to \infty, \dot{\gamma}_0) = \Sigma(\dot{\gamma}_0)$. The criterion for shear banding (with the constraint now removed) is well known in this limit: that the constitutive curve has a region of negative slope, $d\Sigma/d\dot{\gamma}_0 < 0$. Less artificially, this criterion also marks the onset of a linear instability to the formation of shear bands in an experiment in which the shear rate is very slowly swept upwards from zero.

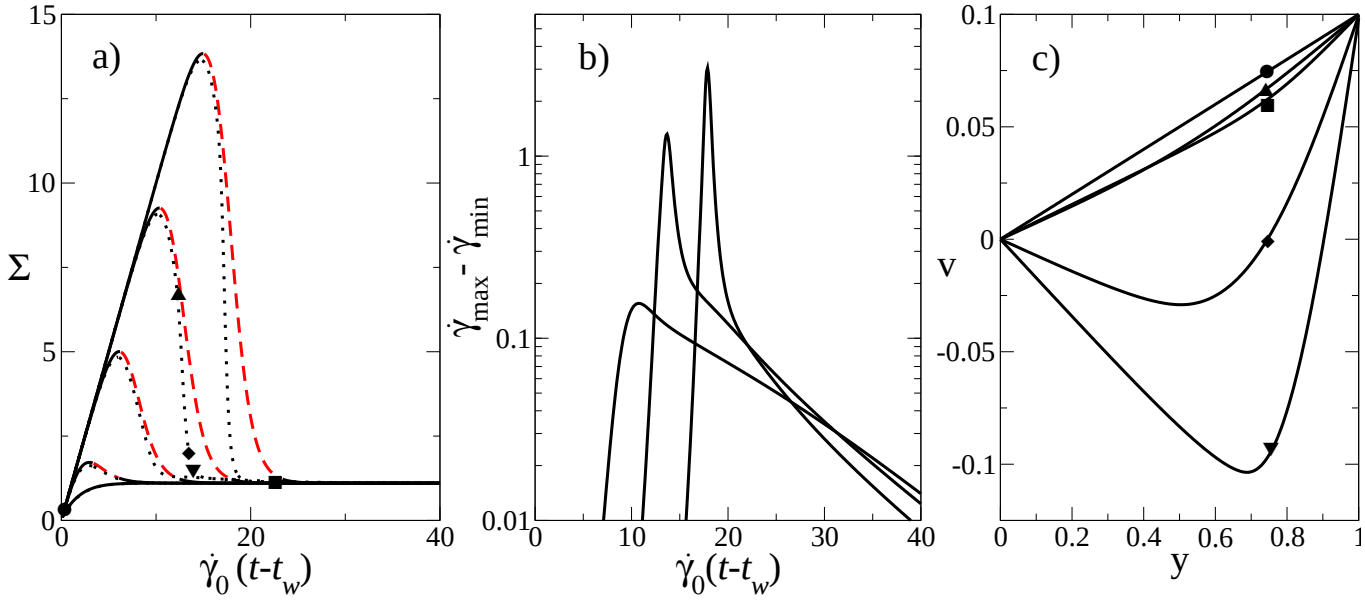


FIG. 3. a) Stress startup curves of the fluidity model for an imposed shear rate $\dot\gamma_0 = 0.1$ and different initial sample ages $t_w = 10^0, 10^2, 10^4, 10^6, 10^8$ (curves upwards). Thick lines: homogeneously constrained run, with dashed regions denoting regimes of linear instability to the onset of banding. Dotted lines: full heterogeneous simulation with banding allowed. b) Corresponding degree of shear banding for $t_w = 10^4, 10^6, 10^8$ (in order of increasing peak height). c) Velocity profiles at times denoted by corresponding symbols in a). Parameters: $\eta = 0.005, l_0 = 0.01, \delta = 0.01$.

Because the fluid flows in a liquid-like way in this steady state limit, we refer to this type of banding, triggered by a regime of declining stress versus strain rate $d\Sigma/d\dot\gamma_0 < 0$, as 'viscous' for convenient nomenclature in what follows. As already discussed, the SGR and fluidity models (at least in their form as introduced above) each have a monotonic constitutive curve $d\Sigma/d\dot\gamma_0 > 0$ and so do not capture steady state viscous banding.

The viscous banding scenario just discussed is analogous to but distinct from a similar instability known to arise in nonlinear elastic solids that are subject to an applied shear strain. In this case, a state of initially homogeneous shear deformation undergoes an 'elastic' instability to the formation of coexisting bands of differing strain in any regime in which the stress is a declining function of the applied strain, $d\Sigma/d\gamma_0 < 0$.

Besides providing an interesting analogy, this elastic instability in fact has directly important implications for viscoelastic fluids as well. Consider a shear startup run performed in the limit of a flow rate $\dot\gamma_0 \to \infty$ that exceeds the fluid's intrinsic viscoelastic stress relaxation rates. In this regime, many viscoelastic materials attain a limiting startup curve $\Sigma(\gamma_0, \dot\gamma_0 \to \infty) = \Sigma(\gamma_0)$ that depends only on strain, independent of the strain rate, at least while the accumulated strain remains modest. Once the imposed $\dot\gamma_0$ exceeds the material's intrinsic relaxation rates, then, performing the run at any higher $\dot\gamma_0$ would give the same startup curve $\Sigma(\gamma_0)$. In this regime, $\gamma_0$ can be thought of as an elastic strain variable and the material essentially behaves as a nonlinear elastic solid. If this limiting curve furthermore shows an overshoot followed by a regime of declining stress $d\Sigma/d\gamma_0 < 0$, we expect elastic banding to arise during startup.

Precisely this scenario was explored in the context of fast shear startup experiments in polymeric fluids in Refs.[34,79], with an elastic banding instability being shown to set in around the time of the stress overshoot. If the fluid furthermore has negative slope in its underlying constitutive curve $d\Sigma/d\dot\gamma_0 < 0$, these elastic bands can be thought of as the formative precursor of viscous bands that will persist to steady state $\gamma_0 \to \infty$. In contrast, for a fluid with a monotonic constitutive curve the elastic bands persist only transiently during startup, eventually decaying to leave homogeneous shear flow in the final steady state.

Soft glassy materials typically also show a strong stress overshoot in startup, separating an early time elastic regime in which the stress grows linearly with the accumulated strain $\Sigma = G\gamma_0$, from a final steady state in which the stress is prescribed by a balance between elastic loading and plastic relaxation. In these materials, however, the overshoot cannot be attributed a purely elastic origin because the decrease in stress post-overshoot arises directly from the onset of the plastic relaxation processes that lead to the eventual steady flowing state. Accordingly, $\gamma_0$ is not an elastic strain variable in the regime

where $d\Sigma/d\gamma_0 < 0$, and there can be no direct mapping to an elastic banding scenario. Soft glasses have nonetheless been shown to exhibit pronounced banding in startup, which furthermore does appear closely associated with stress overshoot, as surveyed in Sec. II above. Motivated by these observations, we now discuss shear startup in the fluidity and SGR models, following Ref.[35].

As already discussed, the onset of banding in a time-dependent flow protocol can be predicted by considering an underlying time-evolving base state of homogeneous shear response to the imposed deformation, then studying the dynamics of heterogeneous perturbations to this base state (both at the level of linear instability while the perturbations remain small, then nonlinear dynamics once noticeable bands have developed later on). In what follows, therefore, we shall first consider the stress startup curves of the fluidity and SGR models with an artificially imposed constraint of homogeneous shear in each case. (As noted above these must also coincide with the startup curves measured experimentally, at least until any significant banding arises.) We shall then demonstrate that the presence of an overshoot in the startup curve is closely associated with the onset of an instability to the formation of shear bands in a model that does allow spatial variations, and accordingly also experimentally.

Startup curves $\Sigma(\gamma_0, \dot{\gamma}_0)$ of the fluidity model are shown in Fig. 3a) for several different sample ages $t_w$, for a base state flow that is constrained to remain homogeneous. These display an overshoot that depends strongly on the sample age $t_w$, occurring at a strain $\gamma_0 = \log(\dot{\gamma}_0 t_w)$ (to within logarithmic corrections) and a corresponding stress $\Sigma_0 \approx G \log(\dot{\gamma}_0 t_w)$. (Experimentally, however, the functional form is often observed to be a weak power law[17,57].) As discussed above, the presence of an overshoot followed by a regime of declining stress $d\Sigma/d\gamma_0 < 0$ is expected to give rise to the formation of shear bands. A linear stability analysis of the dynamics of small heterogeneous perturbations about the evolving homogeneous base state indeed confirms this, with a regime of instability indicated by the red dashed lines Fig. 3a.

As can be seen, the regime of instability is much more pronounced for larger values of the waiting time $t_w$, consistent with the degree of instability being controlled by the size of the overshoot, which is much larger in samples that were first aged into a more elastic state before the flow commenced. Accordingly, we expect much more pronounced transient banding to arise in samples that are left for a long time after preparation before the startup of flow. In young samples, in contrast, any region of instability will be sufficiently weak and short lived that no observable banding can develop during startup.

With these considerations in mind, we now turn to the full heterogeneous dynamics of the fluidity model, performing nonlinear simulations that also allow for spatial variations in the flow gradient direction $y$. Each run is initialised with a small perturbation $\sigma(y, t = 0) = \delta \cos(\pi y)$ with $\delta \ll 1$, in order to seed any banding. As a function of shearing time $t - t_w$ (or equivalently of accumulated strain $\dot{\gamma}_0(t - t_w)$) we then track the degree of shear banding across the sample, which we measure at any instant by the difference $\dot{\gamma}_{\max} - \dot{\gamma}_{\min}$ between the maximum and minimum shear rates present in the cell. The evolution of this quantity is shown in Fig. 3b. Regimes of high $\dot{\gamma}_{\max} - \dot{\gamma}_{\min}$ indeed match up with those of negative slope in the startup curves, and with much more pronounced transient banding for the older samples, as anticipated above.

Snapshots of the bands at representative times during one run are shown in Fig. 3, and indeed exhibit pronounced shear banding. Note that the shear rate in the low shear rate band in fact becomes negative during startup, consistent with this band responding essentially like an elastic slab subject to a declining stress post-overshoot: an elastic material being unloaded will indeed shear backwards. At longer times the bands decay to leave the flow homogeneous in the final steady state, consistent with the underlying constitutive curve of the model being monotonic in a simple YSF, $d\Sigma/d\dot{\gamma}_0 > 0$.

This transient formation of shear bands also slightly perturbs the startup curves in Fig. 3a, leading to a reduced stress relative to that of the homogeneous startup flow. The overall shape of the curves is however qualitatively unaffected. This is consistent with our claim made above, that bulk rheological data can be used as predictor of the presence of shear banding within the sample, even in the absence of spatially resolved velocimetry.

The same overall behaviour is seen in the SGR model, with an age-dependent stress overshoot triggering the formation of pronounced transient shear banding during startup (not shown). The same was also seen in a model of shear transformation zones[38] and in an elasto-plastic model[44]. The observation of the same behaviour in four different models leads us to suggest that shear banding associated with startup overshoot must arise generally in soft glassy materials that have been aged prior to shear.

There is however a new feature in the SGR model, not seen in the fluidity model. For the oldest samples the time scale for the bands to decay back to a homogeneous flow can be inordinately long, requiring thousands of strain units. (Not shown; see Ref.[35] for details.) Indeed such strains may be unattainable in any realistic experiment, in which case shear banding would represent the ultimate flow response of the material for practical purposes, even though the underlying constitutive curve of the material is monotonic and any true steady state homogeneous. (Because strain in general rejuvenates a soft glass, this long lifespan of the low shear band is possible only because the strain rate in it remains extremely small compared to the average shear rate applied to the sample as a whole.) We return in Sec. VI below to discuss the implications of such long-lived bands, even with a monotonic constitutive curve, for the apparent distinction between simple YSFs and viscosity-bifurcating YSFs that is widely discussed in the experimental literature.

As noted above, in soft glasses the presence of a stress

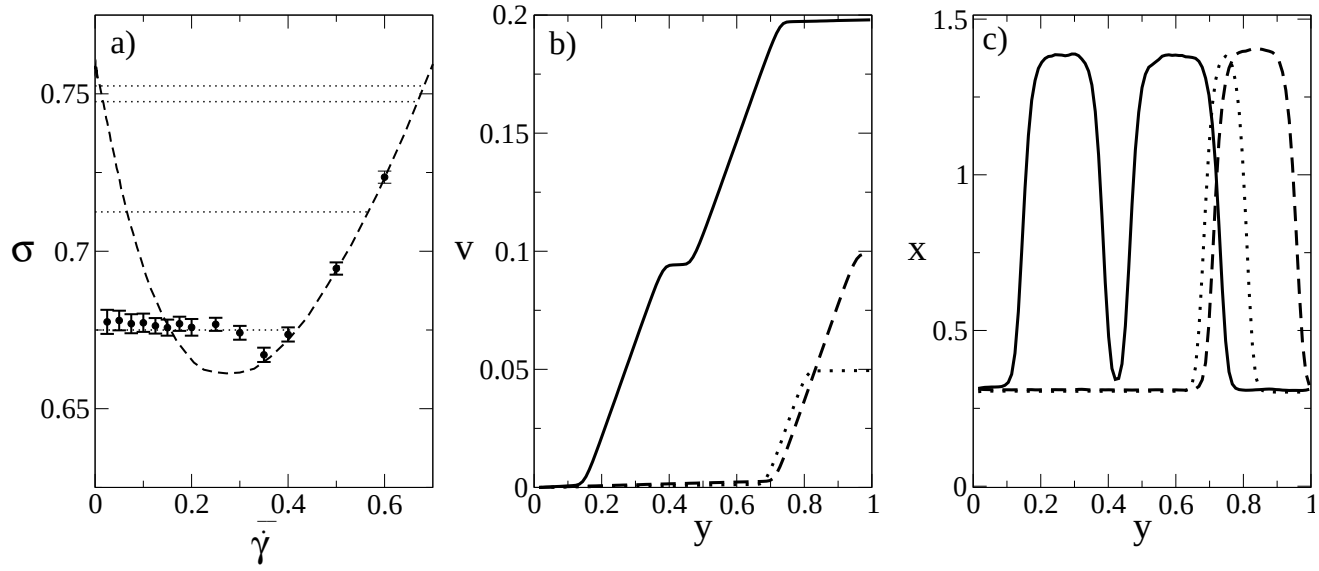


FIG. 4. a) Dashed line: constitutive curve of stress against strain rate for homogeneous shear states of model 1 for $x_0 = 0.3$, $a = 2.0$. Symbols: stress at various mean imposed shear rates $\bar{\dot{\gamma}}$ found in the long time limit after startup of steady shear. Shear banding is present in any regime where the symbols differ significantly from the constitutive curve. b) Velocity profiles for imposed mean shear rates $\bar{\dot{\gamma}} = 0.05, 0.1, 0.2$ (dotted, dashed, solid). c) Corresponding profiles of noise temperature.

overshoot during shear startup arises from a competition between elastic loading and plastic relaxation. In consequence there can be no direct mapping either to a purely elastic instability, $d\Sigma/d\gamma_0 < 0$, or a purely viscous instability, $d\Sigma/d\dot{\gamma}_0 < 0$: the instability reported here represents an interesting new intermediate between these two limiting cases.

The predictions reported in this section are consistent with observations of transient shear banding triggered by stress overshoot during shear startup in a simple YSF in Refs.[55,57], which decays to leave homogeneous flow in steady state. In fact our predictions for an initial onset of shear banding triggered by stress overshoot are also consistent with data in viscosity-bifurcating YSF in Ref.[24], and in that case the bands persists permanently, as long as the flow remains applied, consistent with the more complex rheology of viscosity-bifurcating YSFs. It is to these permanent bands in viscosity-bifurcating YSFs that we now turn.

## V. VISCOSITY-BIFURCATING YIELD STRESS FLUIDS

In its form as described so far, the SGR model has a monotonic underlying constitutive curve $\Sigma(\dot{\gamma})$ and does not admit permanent banding under conditions of a steady applied shear flow. This apparently contradicts experimental observations in viscosity-bifurcating YSFs[23–25,30,31] (though see comments in the closing section VI below). This failure of the SGR model to admit non-monotonic constitutive curves may be linked to the fact that its noise temperature $x$ is taken to be a constant parameter of the model. In practice, however, $x$ is not the true temperature but represents in a mean field way coupling between yield events occurring in different parts of the sample. As such, the effective noise temperature experienced by any given element should in fact depend on the level of hopping activity within that element's local vicinity.

With this physical picture in mind, we now move beyond our assumption of a constant $x$ to consider the following picture of relaxation-diffusion dynamics:

$$\tau_x \dot{x}(y,t) = -x + x_0 + S + \lambda^2 \frac{\partial^2 x}{\partial y^2} = 0. \qquad (13)$$

In the second equality we have for simplicity set $\tau_x \to 0$ so that the noise temperature rapidly adapts to changes in nearby activity levels.

The diffusive term in this equation obviates the need for any stochastic diffusive dynamics of the kind discussed at the end of Sec. III A above, so we henceforth set the parameter $w$ introduced in that section to zero. Besides these changes, the model is otherwise unchanged from the dynamics defined previously.

The source term $S(y)$ in Eqn. 13 represents pumping of the noise by hopping events, and so depends on the probability distribution $P(E, l, y, t)$ at position $y$. We henceforth denote this $P(y)$ for notational convenience. In

what follows we shall explore two model variants, based on different choices for this source term.

- Model 1 has

$$S(y) = a\langle l^2/\tau\rangle_{P(y)}, \tag{14}$$

where $\tau = \tau_0 \exp\left[(E - kl^2/2)/x\right]$ is the trap lifetime. Within this choice, the noise is assumed to be pumped by the dissipation of elastic energy.

- Model 2 instead has

$$S(y) = \tilde{a}\langle 1/\tau\rangle_{P(y)}, \tag{15}$$

in which all hops contribute equally to the noise, regardless of the local strain released in any hop.

We first explore our results for model 1. In a homogeneous steady state, Eqns. 13 and 14 are together equivalent to

$$x = x_0 + 2a\Sigma(x, \dot{\gamma})\dot{\gamma}. \tag{16}$$

This implicit relation allows us to construct the homogeneous constitutive curve $\Sigma(\dot{\gamma})$, for any $x_0$ and $a$, as a composite combination of the constant-$x$ curves of the original model in Fig. 1. See the dashed line in Fig. 4a). As can be seen, the constitutive curve now has non-zero yield stress $\Sigma_y$ in the limit $\dot{\gamma} \to 0$, followed by a region of declining stress $d\Sigma/d\dot{\gamma} < 0$, before restabilising at higher shear rates. In a step stress protocol, this gives rise to a classic viscosity-bifurcation scenario: see Fig. 3 of Ref.[36].

This nonmonotonicity also creates the standard preconditions for permanent shear banding under conditions of a constant imposed shear rate. Unusually, however, compared with more familiar ergodic shear banding fluids such as wormlike micelles, the presence of a yield stress in Fig. 4 implies that the viscous band will be effectively unsheared. A waiting time Monte Carlo simulation of the model's full spatio-temporal dynamics confirms this scenario: see Fig. 4. The low shear band is indeed effectively solid, with a strain rate close to zero and a low noise temperature $x \approx x_0 = 0.3$ such that $\Sigma_{\rm y}(x) > \Sigma$. Under these conditions, ergodicity is broken in this low shear band and the dynamical correlator $C(t, t_w)$, which measures the fraction of unhopped particles, exhibits simple aging when measured locally in this band (not shown). In contrast, the high-shear band has a high level of activity that self-consistently maintains it in an ergodic state of high $x$ and low viscosity. Plotting the stress as a function of the overall imposed shear rate $\bar{\dot{\gamma}}$ in this shear banding regime then gives a plateau in the flow curve that is strongly characteristic of shear banded flows. We further find the relative volume fractions of the bands to obey a lever rule, as seen experimentally[31].

Other theoretical approaches to invoke a nonmonotonic constitutive curve and capture permanent shear banding in steady shear include fluidity models besides the one used here[47,48], models of coupled elastic plastic events[42,43,46] and STZ theories[37]. These findings, and our predictions just discussed, are consistent with experimental reports in viscosity-bifurcating YSFs[23–25,31].

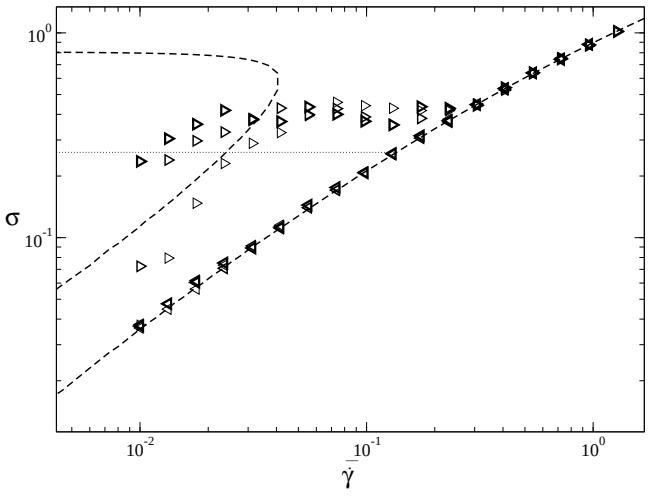


FIG. 5. Dashed lines: constitutive curve of shear stress against shear rate for homogeneous flow states in model 2 with $x_0 = 0.15, \tilde{a} = 3.75$. Symbols: stress values in spatially resolved waiting time Monte Carlo simulations ($n = 100, m = 1000, \lambda = 0.5\Delta$) for up/down strain-rate sweeps (right-pointing and left-pointing triangles respectively) with a residence time per point of $t_r = 200, 400, 800$ (thin, medium, bold symbols). In each run the system was initialized in a homogeneously aged state of $t_w = 10^4$. Dotted line shows, as a guided to the eye, the quasi-steady stress attained at long times in shear startup for $\bar{\dot{\gamma}} \leq 0.1$ in the shear banding regime.

We next turn to Model 2, which, as we shall show, has constitutive curves of a shape that allows us to address recent experiments on star polymers[30,61]. Under conditions of a relatively rapid upward shear-rate sweep (with a residence time $t_{\rm r} = 10s$ per observation point), these materials experimentally show an apparently conventional monotonic flow curve. In contrast, slower sweeps with $t_{\rm r} = 10^4 s$ give a much larger stress that is almost constant at small values of the imposed shear rate. NMR velocimetry reveals the presence of shear banding in this regime, with the viscous band effectively unsheared, $\dot{\gamma} = 0$. A strong hysteresis is also seen, with the less viscous branch persisting to much lower strain rates on sweeping the applied shear rate down towards zero again.

As can be seen in Fig. 5, this experimental scenario is indeed captured by model 2. The right-pointing triangles show the model's stress response to a slow upward shear rate sweep for a sample of age $t_w = 10^4$ before shear. This exhibits an obvious stress plateau for shear rates $\dot{\gamma} < 0.3$, which is the signature of coexisting glassy and flowing shear bands (not shown). (At the lowest applied shear rates, the stress does not have time to attain this plateau stress before the strain rate is swept on to a higher value.) For shear rates $\dot{\gamma} > 0.3$ the system flows homogeneously on the fluid branch of the constitutive curve. A remarkable feature of Model 2, not seen in

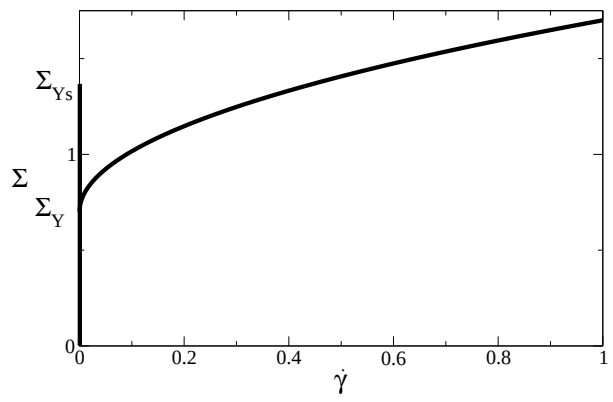


FIG. 6. Sketch of a static yield stress exceeding the dynamic one, allowing a possible coexistence of static and flow shear bands at a common value of the stress.

Model 1, is that the constitutive curve $\Sigma(\dot{\gamma})$ is multivalued, in both stress and strain rate, down to the lowest accessible shear rates. In consequence, after the sample has been in a flowing state on the fluid branch at a high value of $\dot{\gamma}$, it can remain in a homogeneous fluidized state even as the shear rate is ramped back down to zero: see the left-pointing triangles in Fig. 5. This is consistent with the experiments on star polymers in Refs.[30,61].

In this section on viscosity bifurcating YSFs, we have focussed mainly on the permanent shear banding effects that are unique to this class of fluids, and not seen in simple YSFs. Nonetheless, the time-dependent banding effects reported in Sec. IV above for simple YSFs are expected to arise in viscosity-bifurcating YSFs as well. In particular, we anticipate band formation triggered by stress overshoot during shear startup, and now persisting to steady state for shear rates in the plateau regime of the flow curve[24]. We also expect transient shear banding associated with sudden fluidisation under conditions of an imposed step stress in the vicinity of $\Sigma_y$.

## VI. CONCLUSIONS AND OUTLOOK

In this paper, we have reviewed recent theoretical progress in addressing widespread observations of shear banding in soft glassy materials. Following introductory remarks in Sec. I, we started in Sec. II by surveying the experimental phenomenology, considering in particular a distinction that is widely discussed in the literature: between viscosity-bifurcating yield stress fluids (YSFs), which apparently display permanent shear banding under conditions of a steady applied shear flow, and simple YSFs, in which shear bands arise only transiently during the process whereby a steady flowing state is established out of an initial rest state. (We also noted that viscosity-bifurcating YSFs are often referred to as thixotropic YSFs in the literature, but cautioned against this nomenclature on account of the fact that simple YSFs can also display ageing and rejuvenation effects – *i.e.*, thixotropy – in their time-dependent rheology.)

In Sec. III we introduced the models to be used throughout the paper: the soft glassy rheology (SGR) model and a simple fluidity model. In original form, these both have a monotonic constitutive relation between shear stress and shear rate (for an underlying base state of homogeneous shear flow) and are therefore unable to capture permanent shear banding under conditions of a steady applied shear flow. They do nonetheless convincingly capture observations of shear banding in time-dependent flow protocols such as shear startup and step stress: recall Sec. IV. Although technically only transient, these bands may persist for several hundreds or even thousands of strain units and so represent the ultimate flow response of the material for practical purposes, even in a simple YSF for which the true steady state would in principle be unbanded.

We also discussed these results in the broader context of recently predicted criteria for the onset of shear banding in time-dependent flow protocols[34]. (These criteria in fact apply to all complex fluids, and not just the soft glassy materials of interest here. A detailed investigation of the directly analogous phenomena in ergodic complex fluids such as polymers and wormlike micellar surfactants can be found in Ref.[79].) An important prediction of this work is that shear banding should arise generically in any system where stress overshoots arise in shear startup, and where the time-differentiated creep curve shows a regime of upward curvature following the imposition of a step stress. It could therefore be well worth testing for the existence of shear banding in mode coupling theories[91,92], in Brownian simulations of hard sphere suspensions[91,93], and in experiments on colloidal glasses[81,92,93]. Eventually, one may also wish to consider other time-dependent protocols, besides the case of shear startup and step stress reported here.

With regards flow heterogeneity triggered by upward curvature in the time-differentiated creep curve following the imposition of a step stress, is is interesting to note that two separate regions of upward curvature are observed experimentally in Fig. 1 of Ref.[32]: the first corresponding to a regime of total wall-slip and the second to transient shear banding. Whether total wall-slip could be decsribed in terms of a shear banding-like instability near the walls, and how to incorporate wall effects into SGR and fluidity models, remains an open question.

To address the possibility of permanent shear banding under conditions of a steady applied shear flow, as seen in viscosity-bifurcating YSFs, we introduced in Sec. V a simple variant of the SGR model in which the noise temperature responds dynamically to the local rate of activity. This captures a non-monotonic constitutive curve and so allows permanent banding in a steady applied shear flow. A non-monotonic variant of the fluidity model does likewise, as explored in Refs.[47,48].

As seen in Fig. 4, the form of the non-monotonicity (in model variant 1) comprises a branch of zero-flow states for stresses $\Sigma < \Sigma_y$, followed by a branch of flow states in which the stress first decreases with strain rate before rising again in faster flows. Molecular dynamics studies[49–52] elsewhere in the literature suggest instead the existence of a static yield stress $\Sigma_{Ys}$ below which there exists (for a previously unsheared sample) a branch of zero flow states, with $\Sigma_{Ys}$ exceeding the dynamical yield stress $\Sigma_Y$ as measured in a protocol that instead sweeps the shear rate down towards zero. (That dynamical branch of the constitutive curve is itself purely monotonic.) This gives rise to a downwards step discontinuity (non-monotonicity) in the material's constitutive properties at $\dot{\gamma} = 0$, allowing the coexistence of an unsheared band with a flowing one. See Fig. 6.

In Ref.[52] it was suggested that this difference between $\Sigma_{Ys}$ and $\Sigma_Y$, which gives rise to the discontinuity just described, may persist only for a finite (but very long) duration, and only in a system of finite size (disappearing for an infinitely large system). Indeed, the shear bands observed in that study were very long lived, but not a true zero-frequency phenomenon. Indeed this scenario may not be entirely distinct from the observation of extremely long lived (though technically transient) shear bands in the original SGR model.

Taken together, these considerations raise the intriguing possibility that the apparent difference between a viscosity-bifurcating YSF and a simple YSF might in some cases lie not in a true zero-frequency difference in the structure of their constitutive curves, but rather in the presence of inordinately long (not nonetheless still finite) timescales in viscosity-bifurcating YSFs, which in simple YSFs are instead merely shorter and more commensurate with experimental timescales. Indeed, dialing progressively more attractive particle interactions into the simulations Ref.[52] appeared to increase the window of shear rates affected by $\Sigma_{Ys}$, leading to correspondingly more pronounced and longer lived bands. This question of true non-monotonicity versus transient apparent non-monotonicity clearly deserves further careful thought.

A possible mechanism for true steady state shear banding *without* a non-monotonic constitutive curve is that of coupling between flow and concentration fluctuations, via normal stresses. This has long been known to arise in polymer and wormlike micellar surfactant solutions, and was explored in the context of steady shear banded states colloidal glasses in Ref.[90], in a theoretical description not related to the SGR model. (Indeed, the SGR model in its present form does not allow for concentration fluctuations.)

Transient shear banding during time-dependent shear in a polymer glass was recently reported theoretically in Ref.[94]. Clearly, it would be interesting to explore in more detail spatially heterogeneous deformation of polymer glasses both theoretically and experimentally.

Finally, an effect that arises virtually ubiquitously in the rheology of complex fluids is that of wall slip: reports are widespread in the experimental literature, ranging from the anecdotal to the carefully considered. The drastic effect of boundary conditions and wall slip on yielding phenomena was reported in particularly careful detail in Refs.[95,96]. Clearly, any manifestations of wall slip become increasingly more important in confined geometries, as do any non-local effects in the fluid's rheological properties[97,98]. Detailed theoretical studies of both wall slip (which is unaccounted for by the SGR and fluidity models in their present form) and non-locality remain open challenges for the future.

## VII. ACKNOWLEDGEMENTS

The author thanks Mike Cates, Robyn Cooke (née Moorcroft) and Peter Sollich for helpful discussions and enjoyable collaboration on these topics. The research leading to these results has received funding from the European Research Council under the European Union's Seventh Framework Programme (FP7/2007- 2013) / ERC Grant agreement no. 279365; and from the UK's EPSRC (EP/E5336X/1).

The author dedicates this manuscript to the memory of Professor Sir Paul Callaghan.

[1] S. D. Holdsworth, Trans. Inst. Chem. Eng. **71**, 139 (1993).
[2] H. A. Barnes, J. F. Hutton, and K. Walters, *An introduction to rheology* (Elsevier, Amsterdam, 1989).
[3] E. Dickinson, *An introduction to food colloids* (Oxford University Press, Oxford, 1992).
[4] R. J. Ketz, R. K. Prudhomme, and W. W. Graessley, Rheol. Acta **27**, 531 (1988).
[5] S. A. Khan, C. A. Schnepper, and R. C. Armstrong, J. Rheol. **32**, 69 (1988).
[6] T. G. Mason and D. A. Weitz, Phys. Rev. Lett. **75**, 2770 (1995).
[7] T. G. Mason, J. Bibette, and D. A. Weitz, Phys. Rev. Lett. **75**, 2051 (1995).
[8] P. Panizza, D. Roux, V. Vuillaume, C. Lu, and M. Cates, LANGMUIR **12**, 248 (1996).
[9] R. Hohler, S. Cohen-Addad, and A. Asnacios, EUROPHYSICS LETTERS **48**, 93 (1999).
[10] M. Cloitre, R. Borrega, and L. Leibler, PHYSICAL REVIEW LETTERS **85**, 4819 (2000).
[11] L. Cipelletti and L. Ramos JOURNAL OF PHYSICS-CONDENSED MATTER **17** R253-R285 (2005).
[12] G. Ovarlez and P. Coussot, PHYSICAL REVIEW E **76** 011406 (2007).
[13] A. S. Negi, and C. O. Osuji, PHYSICAL REVIEW E **80** 010404 (2009).
[14] P. Moller, A. Fall, V. Chikkadi, D. Derks and D. Bonn Phil. Trans. R. Soc. A. **367** 5139-5155 (2009).
[15] T. Gibaud, C. Barentin, N. Taberlet, et al., Soft Matter, **5**, 3026-3037 (2009).
[16] V. Gopalakrishnan and C. F. Zukoski, JOURNAL OF RHEOLOGY **51** 623-644 (2007).
[17] C. Derec, G. Ducouret, A. Ajdari, et al. PHYSICAL REVIEW E **67** 061403 (2003).
[18] S. Cohen-Addad and R. Hohler, PHYSICAL REVIEW LETTERS **86**, 4700 (2001).
[19] V. Viasnoff and F. Lequeux, PHYSICAL REVIEW LETTERS **89**, 065701 (2002).
[20] V. Viasnoff, S. Jurine, and F. Lequeux, FARADAY DISCUSSIONS **123**, 253 (2003), General Meeting on Non-Equilibrium

Behaviour of Colloidal Dispersions, EDINBURGH, SCOTLAND, SEP 09-11, 2002.
[21] M. Cloitre, R. Borrega, F. Monti, and L. Leibler, PHYSICAL REVIEW LETTERS **90**, 068303 (2003).
[22] P. Sollich, F. Lequeux, P. Hebraud, and M. Cates, PHYSICAL REVIEW LETTERS **78**, 2020 (1997).
[23] P. Coussot, Q. D. Nguyen, H. T. Huynh, and D. Bonn, Phys. Rev. Lett. **88**, 175501 (2002).
[24] J. D. Martin and Y. T. Hu, Soft Matter **8**, 6940 (2012).
[25] J. Paredes, N. Shahidzadeh-Bonn, and D. Bonn, J. Physics-condensed Matter **23**, 284116 (2011).
[26] L. Becu, S. Manneville, A. Colin, PHYSICAL REVIEW LETTERS **96** 138302 (2006).
[27] G. Ovarlez, S. Rodts, A. Ragouilliaux, et al., PHYSICAL REVIEW E **78** 036307 (2008).
[28] G. Ovarlez, S. Cohen-Addad, K. Krishan, K. et al. JOURNAL OF NON-NEWTONIAN FLUID MECHANICS **193** 68-79 (2013).
[29] M. Dennin, JOURNAL OF PHYSICS-CONDENSED MATTER **20** 283103 (2008).
[30] S. A. Rogers, D. Vlassopoulos, and P. T. Callaghan, Phys. Rev. Lett. **100**, 128304 (2008).
[31] P. C. F. Moller, S. Rodts, M. A. J. Michels and D. Bonn, Phys. Rev. E **77**, 041507 (2008).
[32] T. Divoux, C. Barentin, and S. Manneville, SOFT MATTER **7**, 8409 (2011).
[33] T. Gibaud, D. Frelat, and S. Manneville, SOFT MATTER **6**, 3482 (2010).
[34] R. L. Moorcroft and S. M. Fielding, Phys. Rev. Lett. **110**, 086001 (2013).
[35] R. L. Moorcroft, M. E. Cates, and S. M. Fielding, PHYSICAL REVIEW LETTERS **106**, 055502 (2011).
[36] S. M. Fielding, M. E. Cates, and P. Sollich, SOFT MATTER **5**, 2378 (2009).
[37] M. L. Manning, E. G. Daub, J. S. Langer, and J. M. Carlson, Phys. Rev. E **79**, 016110 (2009).
[38] M. L. Manning, J. S. Langer, and J. M. Carlson, Phys. Rev. E **76**, 056106 (2007).
[39] M. L. Falk and J. S. Langer, Ann. Rev. Condensed Matter Physics, Vol 2 **2**, 353 (2011).
[40] G. Picard, A. Ajdari, F. Lequeux, and L. Bocquet, European Phys. J. E **15**, 371 (2004).
[41] G. Picard, A. Ajdari, F. Lequeux, and L. Bocquet, Phys. Rev. E **71**, 010501(R) (2005).
[42] V. Mansard, A. Colin, P. Chauduri, and L. Bocquet, Soft Matter **7**, 5524 (2011).
[43] K. Martens, L. Bocquet, and J.-L. Barrat, Soft Matter **8**, 4197 (2012).
[44] E. A. Jagla, J. Statistical Mechanics-theory Experiment P12025 (2010).
[45] L. Bocquet, A. Colin, and A. Ajdari, Phys. Rev. Lett. **103**, 036001 (2009).
[46] E. A. Jagla, Phys. Rev. E **76**, 046119 (2007).
[47] G. Picard, A. Ajdari, L. Bocquet, and F. Lequeux, Phys. Rev. E **66**, 051501 (2002).
[48] P. Coussot, Q. D. Nguyen, H. T. Huynh, and D. Bonn, J. Rheology **46**, 573 (2002).
[49] F. Varnik, L. Bocquet, J. L. Barrat, and L. Berthier, Phys. Rev. Lett. **90**, 095702 (2003).
[50] F. Varnik, L. Bocquet, and J. L. Barrat, J. Chem. Phys. **120**, 2788 (2004).
[51] N. Xu and C. S. O'Hern, Phys. Rev. E **73**, 061303 (2006).
[52] P. Chaudhuri, L. Berthier, and L. Bocquet, Phys. Rev. E **85**, 021503 (2012).
[53] J. Paredes, M. A.J. Michels, and D. Bonn, Phys. Rev. Lett. **111**, 015701 (2013).
[54] A. Ragouilliaux, G. Ovarlez, N. Shahidzadeh-Bonn, B. Herzhaft, T. Palermo, and P. Coussot, Phys. Rev. E **76**, 051408 (2007).
[55] T. Divoux, D. Tamarii, C. Barentin, and S. Manneville, Phys. Rev. Lett. **104**, 208301 (2010).
[56] T. Divoux, V. Grenard, and S. Manneville, Phys. Rev. Lett. **110**, 018304 (2013).
[57] T. Divoux, C. Barentin, and S. Manneville, Soft Matter **7**, 9335 (2011).
[58] P. C. F. Moller, A. Fall, and D. Bonn, Europhysics Letters **87**, 38004 (2009).
[59] G. Ovarlez, K. Krishanand S. Cohen-Addad, Europhysics Letters **91** 68005 (2010).
[60] F. D. Cruz, F. Chevoir, D. Bonn, and P. Coussot, Phys. Rev. E **66**, 051305 (2002).
[61] S. A. Rogers, P. T. Callaghan, G. Petekidis, and D. Vlassopoulos, J. Rheology **54**, 133 (2010).
[62] P. E. Boukany and S.-Q. Wang, SOFT MATTER **5**, 780 (2009).
[63] P. E. Boukany and S.-Q. Wang, MACROMOLECULES **43**, 6950 (2010).
[64] S. Ravindranath, S.-Q. Wang, M. Ofechnowicz, and R. P. Quirk, MACROMOLECULES **41**, 2663 (2008).
[65] P. Tapadia and S. Q. Wang, Phys. Rev. Lett. **96**, 016001 (2006).
[66] P. E. Boukany and S.-Q. Wang, MACROMOLECULES **41**, 1455 (2008).
[67] M. E. Helgeson, M. D. Reichert, Y. T. Hu, and N. J. Wagner, Soft Matter **5**, 3858 (2009).
[68] M. E. Helgeson, P. A. Vasquez, E. W. Kaler, and N. J. Wagner, J. Rheol. **53**, 727 (2009).
[69] Y. T. Hu, C. Palla, and A. Lips, Journal of Rheology **52**, 379 (2008).
[70] J. P. Decruppe, S. Lerouge, and J. F. Berret, Phys. Rev. E **63**, 022501 (2001).
[71] S. Lerouge, M. A. Fardin, M. Argentina, G. Gregoire, and O. Cardoso, Soft Matter **4**, 1808 (2008).
[72] J. Decruppe, O. Greffier, S. Manneville, and S. Lerouge, Physical Review E **73**, 061509 (2006).
[73] M. M. Britton and P. T. Callaghan, Phys. Rev. Lett. **78**, 4930 (1997).
[74] M. M. Britton and P. T. Callaghan, European Phys. J. B **7**, 237 (1999).
[75] R. W. Mair and P. T. Callaghan, Europhys. Lett. **36**, 719 (1996).
[76] E. Miller and J. Rothstein, Journal Of Non-Newtonian Fluid Mechanics **143**, 22 (2007).
[77] J. B. Salmon, A. Colin, S. Manneville, and F. Molino, Phys. Rev. Lett. **90**, 228303 (2003).
[78] R. L. Cooke, Durham theses, Durham University (2013). Available at Durham E-theses online: http://etheses.dur.ac.uk/7285/
[79] R. L. Moorcroft and S. M. Fielding, Journal of Rheology 58 **103** (2014).
[80] F. Caton and C. Baravian, Rheologica Acta **47**, 601 (2008).
[81] M. Siebenbuerger, M. Ballauff, and T. h. Voigtmann, Phys. Rev. Lett. **108**, 255701 (2012).
[82] J. Sprakel, S. B. Lindstroem, T. E. Kodger, and D. A. Weitz, Phys. Rev. Lett. **106**, 248303 (2011).
[83] T. Bauer, J. Oberdisse, and L. Ramos, Phys. Rev. Lett. **97**, 258303 (2006).
[84] E. N. da C. Andrade, Proceedings of the Royal Society of London. Series A **84**, 567 (1910).
[85] J. L. Goveas and P. D. Olmsted EUROPEAN PHYSICAL JOURNAL E **6** 79-89 (2001); C. B .Holmes, M. E. Cates, M. Fuchs and P. Sollich, JOURNAL OF RHEOLOGY **49** 237-269 (2005).
[86] J. P. Bouchaud, J. Phys. (France) I **2**, 1705 (1992).
[87] P. Sollich, PHYSICAL REVIEW E **58**, 738 (1998).
[88] C. Lu, P. Olmsted, and R. Ball, PHYSICAL REVIEW LETTERS **84**, 642 (2000).
[89] S. Fielding, P. Sollich, and M. Cates, JOURNAL OF RHEOLOGY **44**, 323 (2000).
[90] R. Besseling, L. Isa, P. Ballesta, G. Petekidis, M. E. Cates, and W. C. K. Poon, PHYSICAL REVIEW LETTERS **105**, 268301 (2010).
[91] M. Laurati, K. J. Mutch, N. Koumakis, J. Zausch, C. P. Amann, A. B. Schofield, G. Petekidis, J. F. Brady, J. Horbach, M. Fuchs and S. U. Egelhaaf, J. Phys: Condensed Matter **24** 464104

(2012).
[92]C. P. Amann, M. Siebenbuerger, M. Krueger, et al. JOURNAL OF RHEOLOGY **57** 149-175 (2013).
[93]N. Koumakis, M. Laurati, S. U. Egelhaaf, J. F. Brady, and G. Petekidis, Physical Review Letters **108** 098303 (2012).
[94]S. M. Fielding, R. L. Moorcroft, R. G. Larson and M. E. Cates Journal of Chemical Physics **138** 12A504 (2013).
[95]T. Gibaud, C. Barentin, and S. Manneville, Phys. Rev. Lett. **101**, 258302 (2008).
[96]J. R. Seth, C. Locatelli-Champagne, F. Monti, et al. SOFT MATTER **8** 140-148 (2012).
[97]J. Goyon, A. Colin, G. Ovarlez, A. Ajdari, and L. Bocquet, Nature **454**, 84 (2008).
[98]V. Mansard and A. Colin, Soft Matter **8**, 4025 (2012).